Structural Engineering and Mechanics, *Vol. 54, No. 2 (2015) 199-219*
DOI: http://dx.doi.org/10.12989/sem.2015.54.2.199

Condition assessment for high-speed railway bridges based on train-induced strain response

Zhonglong Li[1a], Shunlong Li[*1], Jia Lv[2b] and Hui Li[1c]

[1]School of Transportation Science and Engineering, Harbin Institute of Technology, 73 Huanghe Road, Nangang District, Harbin 150090, People's Republic of China
[2]Harbin Municipal Engineering Design Institute, Building 217, Dafangli, Daowai District, Harbin 150000, People's Republic of China

(Received October 31, 2014, Revised January 6, 2015, Accepted January 9, 2015)

Abstract. This paper presents the non-destructive evaluation of a high-speed railway bridge using train-induced strain responses. Based on the train-track-bridge interaction analysis, the strain responses of a high-speed railway bridge under moving trains with different operation status could be calculated. The train induced strain responses could be divided into two parts: the force vibration stage and the free vibration stage. The strain-displacement relationship is analysed and used for deriving critical displacements from theoretical stain measurements at a forced vibration stage. The derived displacements would be suitable for the condition assessment of the bridge through design specifications defined indexes and would show certain limits to the practical application. Thus, the damage identification of high-speed railways, such as the stiffness degradation location, needs to be done by comparing the measured strain response under moving trains in different states because the vehicle types of high-speed railway are relatively clear and definite. The monitored strain responses at the free vibration stage, after trains pass through the bridge, would be used for identifying the strain modes. The relationship between and the degradation degree and the strain mode shapes shows certain rules for the widely used simply supported beam bridges. The numerical simulation proves simple and effective for the proposed method to locate and quantify the stiffness degradation.

Keywords: condition assessment; train-induced responses; high-speed railway bridges; strain modes; structural health monitoring

1. Introduction

The high-speed railway is one of the great achievements in the world of high technologies and is developing rapidly in many countries. By the end of 2012, the high-speed railway operating mileage in China was 9536 km, and 1330 of 2447 pairs of national railway passenger trains are Electrical Multiple Unit (EMU) Operation Vehicles. China has built the world's longest high-speed

∗Corresponding author, Associate Professor, E-mail: lishunlong@hit.edu.cn
[a]Assistant Professor, E-mail: lizhonglong@hit.edu.cn
[b]Engineer, E-mail: teddy331@qq.com
[c]Professor, E-mail: lihui@hit.edu.cn

http://www.techno-press.org/?journal=sem&subpage=8 ISSN: 1225-4568 (Print), 1598-6217 (Online)

railway systems. With the rapid construction of high-speed railway, it has become a convenient way to travel and plays an important role in China's economic development, national security and daily life.

During long-term service periods, the high-speed railway bridges will endure wind, temperature, humidity, train vehicles, chloride erosion and other environmental loads. Currently, bridge degradation has not been fully understood due to the short operating times (Kim *et al.* 2013). However, the bridge degradation under coupled environmental and train fatigue loads not only influences the structural safety but also threatens traffic safety (Song and Fujino 2008). The failure of high-speed railway bridges will bring enormous social and economic losses and casualties. The condition assessment of high-speed railway bridges will become a huge challenge for service safety in the near future.

An extensive review of the published literature shows that considerable effort regarding railway bridges has focused on the damage identification and fatigue evaluation. Several studies have investigated the effect of train-track-bridge interaction and analysed the dynamic response of railway bridges (Arvidsson *et al.* 2014, Yang *et al.* 2014, Liu *et al.* 2009, Xia and Zhang 2005, Zhang *et al.* 2008, Zhan *et al.* 2011) proposed a dynamic response, sensitivity-based finite element model for an updating damage identification method, which is not only ineffective for detecting local damage of railway bridges but also insensitive to the track irregularity and measurement noise. (Shu *et al.* 2013) implemented a damage detection algorithm based on an Artificial Neural Network (ANN) using the statistical properties of structural dynamic responses as the input for the ANN. (Banjara and Sasmal 2014, Sousa *et al.* 2018, Bruhwiler 2014, Sousa *et al.* 2014, Zhao and Di 2014, Kim *et al.* 2007) studied the fatigue damage of railway bridges under train traffic by investigating the effect of different materials (concrete, steel and composite) and different bridge types (simply supported girder bridge, continuous girder bridge, cable stayed bridge, truss bridge etc.). Previous condition assessment studies on railway bridges have mainly focused on traditional low speed railways. Evaluation methods that consider the characteristics of high-speed railway bridges that endure definite moving loads are limited at present.

This paper presents condition assessment methodology that takes advantage of monitored dynamical strain responses. Fig. 1 summarizes the assessment procedure, which is comprised of two major steps. The first step presents how to acquire high-speed railway bridge responses based on a monitoring system. The structural monitoring systems collect massive amounts of in situ data enabling the identification of train vehicle loads and local strain parameters. In contrast to the common continuous monitoring system, the acquisition strategy for the high-speed railway bridges

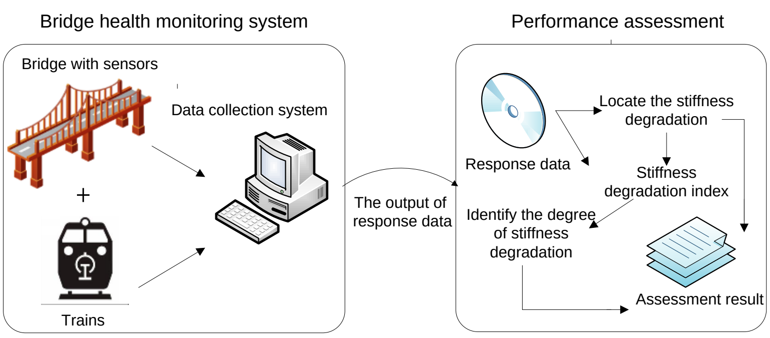

Fig. 1 Condition assessment for bridges based on the health monitoring system

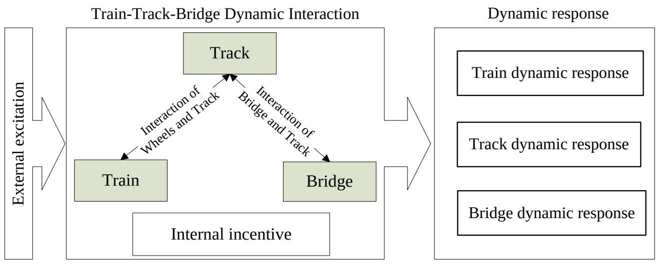

Fig. 2 Flow chart of Train-Track-Bridge dynamic interaction simulation

uses trigger acquisition, meaning that only the dynamic responses when the trains passed through the bridge would be collected. It would be convenient to have the data acquisition system mounted to the high-speed train. In the second step, taking advantage of the monitored responses, the time-variant conditions of the bridge deterioration is presented. The deterioration process of the bridge under both environmental and railway traffic loads is simulated using a stiffness degradation method.

2. Train induced bridge response

2.1 Train-Track-Bridge dynamic interaction

Train-Track-Bridge Dynamic responses mainly consist of three parts, train vibration, track vibration and bridge vibration (Xia *et al.* 2013, Adam and Salcher 2014, Podworna 2011, Rezvani *et al.* 2013, Vieira *et al.* 2014). The three subsystems are coupled into a whole system by the interaction of wheel and track, track and bridge. The flow chart of Train-Track-Bridge dynamic interaction simulation is shown in Fig. 2. In this figure, the external excitations represent wind, earthquake excitation and so on, while the internal incentive demonstrate the geometric deviation of wheels, the serpentine movement of wheels, the track irregularity, etc.

In the Train-Track-Bridge dynamic interaction simulation (Klasztorny 2001), the bridge subsystem is regarded as a flexible body, while the high-speed trains and track are treated as rigid bodies, the coupling type of which is the rigid-flexible coupling. The simulation assumes that the wheel-sets of the vehicles never detach from the bridge and the track irregularity is the only connection between them. Based on the interaction vibration of train-track-bridge system shown in Fig. 1, the equations of coupled motion of the train track and bridge system can be expressed as (Zhang *et al.* 2008, Zhan *et al.* 2011)

$$\mathbf{M}_v\ddot{\mathbf{x}}_v + \mathbf{C}_v\dot{\mathbf{x}}_v + \mathbf{K}_v\mathbf{x}_v = \mathbf{F}_v \tag{1}$$

$$\mathbf{M}_t\ddot{\mathbf{x}}_t + \mathbf{C}_t\dot{\mathbf{x}}_t + \mathbf{K}_t\mathbf{x}_t = \mathbf{F}_t \tag{2}$$

$$\mathbf{M}_b\ddot{\mathbf{x}}_b + \mathbf{C}_b\dot{\mathbf{x}}_b + \mathbf{K}_b\mathbf{x}_b = \mathbf{F}_b \tag{3}$$

where $\mathbf{M}_v$, $\mathbf{C}_v$ and $\mathbf{K}_v$ indicate the mass, damping and stiffness matrices of the train, respectively;

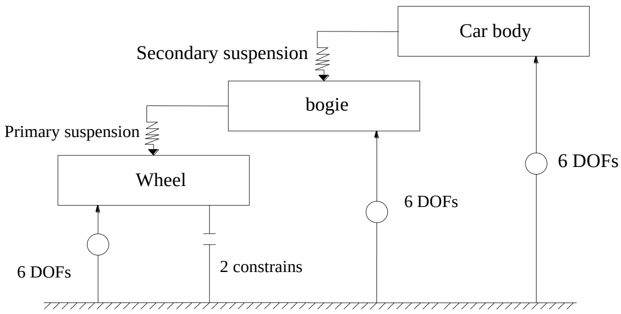

Fig. 3 Schematic diagram of topology relationship for high-speed train

$\mathbf{M}_b$, $\mathbf{C}_b$ and $\mathbf{K}_b$ represent the mass, damping and stiffness matrices of the bridge; $\mathbf{M}_t$, $\mathbf{C}_t$ and $\mathbf{K}_t$ are the mass, damping and stiffness matrices of the track; $\mathbf{x}_v$, $\mathbf{x}_t$ and $\mathbf{x}_b$ demonstrate the generalized displacement vectors of the train, track and bridge; $\mathbf{F}_v$, $\mathbf{F}_t$ and $\mathbf{F}_b$ are the generalized force vectors acting on the train, track and bridge, respectively. The train system (1) and the track system (2) are coupled with the train and track relationship, while the track system (2) and the bridge system (3) are coupled with the bridge and track relationship. When the model parameters and external forces are known (determined by Structural Health Monitoring system and EMU Operation Vehicle type), a large and complex dynamic equation sets can be formulated and solved by Newmark direct integration method. The displacement, velocity and acceleration of location X at time t can be generated from computed nodal responses (Zhan *et al.* 2011).

2.2 High-speed train modelling

Based on the main performance index comparison of high-speed trains used in China and other countries, the EMU Operation Vehicle CRH2 (most commonly used in China), is employed simulate the train-bridge dynamic interaction (CRH is short for China Railway High-speed). The EMU Operation Vehicle CRH2 is the four axis locomotive vehicle model. Each vehicle is composed of car body, bogies, wheel sets and other basic components linked by primary suspension, secondary suspension, vertical damper, longitudinal traction link, torsion spring and other elements. To improve the computational efficiency, these components are usually regarded as a rigid body in the locomotive vehicle dynamics research. To limit the relative movement, there are elastic or rigid constraints among the basic components.

According to the rigid body dynamics, any rigid body has six degrees of freedom (DOF). Each vehicle, for which topological relations are shown in Fig. 3, has a total of 35 DOFs ignoring the longitudinal DOFs of coach.

Standard EMU Operation Vehicle CRH2 adopts eight marshalling, four motor coaches and four trailer coaches, which is divided into two power units. Each power unit is composed of two motor coaches and two trailer coaches (T-M-M-T). The design speed of CRH2 is 200 km/h and the maximum speed reaches 300 km/h. In general, different types of coaches and marshalling of CRH2 is shown as follows

The respective width and total length of the CRH2 is 3.38 m and 201.4 m with 2×25.7 m head coaches and 6×25.0 m middle coaches. The fixed number of passenger is 610 and the maximum and minimum average static axle loads are 140 kN and 11.7 kN, respectively. Detailed information of the designed weights and the geometrical parameters can be seen in Tables 1 and 2.

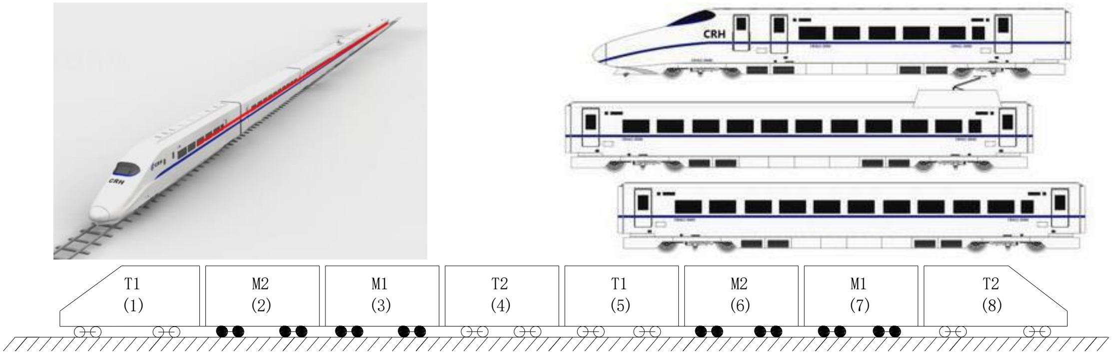

Fig. 4 Marshalling of EMU Operation Vehicle CRH2

Table 1 Geometrical parameters of EMU Operation Vehicle CRH2

Track gauge (mm)	1435	Coach width (mm)	3380	Fixed wheelbase (mm)	2500
Head coach length (m)	25.7	Coach height (mm)	3700	Number of axles	32
Middle coach length (m)	25.0	Bogie pitch (mm)	17500	Wheel diameter (mm)	860
Total length of CRH2 (m)	201.4	Number of bogie	16	Coupler height (mm)	1000

Table 2 Design weights of EMU Operation Vehicle CRH2

Design weights	Coach number								Total
	1	2	3	4	5	6	7	8	
Coach type	T1	M1	M2	T2	T1	M2	M1	T2	
Curb weight (t)	42.8	48	46.5	42	44.1	48	46.8	41.5	359.7(t)
Fixed number of passengers	55	100	85	100	55	100	51	64	610

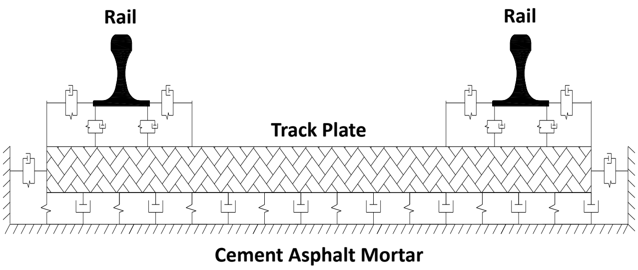

Fig. 5 Mechanics model of ballastless PC slab tracks

2.3 Wheel-rail interaction and track modelling

For the PC slab tracks without ballast, vibration mainly occurs in the rail and track plate, the mechanics model of which can be shown in Fig. 5. The track plate not only fixes and supports rails but also resists and transfers vertical and horizontal loads to the bridge. There are vertical stiffness, lateral stiffness and damping between the track plate and cement asphalt mortar layer. In this study, CRTS III without ballast PC slab track is employed for track simulation, and detailed design parameters are shown in Table 3.

Table 3 Design parameters of CRTS III ballastless PC slab track

Rail	Elastic Modulus (N/m²)	2.06×10^{11}	Track Plate	Elastic Modulus (N/m²)	3.7×10^{10}
	Section inertia (m^4)	3.217×10^{-5}		Width (m)	2.5
	Unit length Mass (kg/m)	60.64		Thickness (m)	0.21
	Poisson ratio	0.3		Density (kg/m^3)	2500
Fastener	Vertical Stiffness (N/m)	5.0×10^{7}	Support Layer	Poisson ratio	0.2
	Vertical Damping (N·s/m)	75000		Stiffness (N/m)	6.0×10^{10}
	Distance (m)	0.63		Damping (N·s/m)	1.0×10^{5}

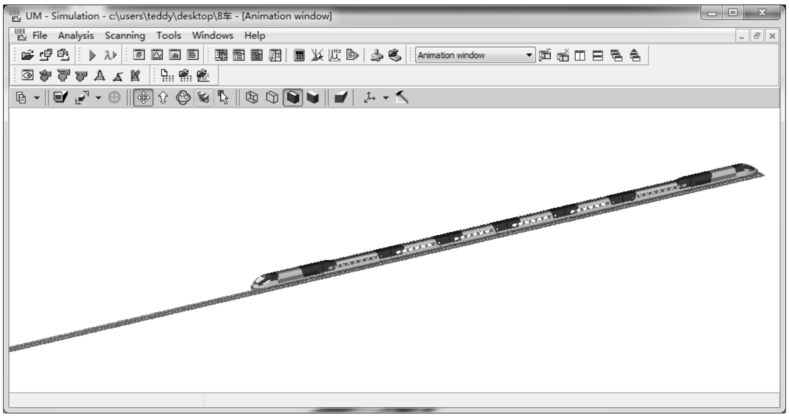

Fig. 6 Multi-rigid-body dynamics model of CRH2 and CRTS III ballastless PC slab tracks

The track force mainly consists of vertical force, lateral force and longitudinal force during the high-speed train operation process. In this study, the vertical force is the major consideration because the vertical force is generally the weight of the vehicle wheels, which has a great influence on the mechanical properties of the bridge structure. Although dynamical wheel loads vary with the train speed, track type, and operation status, its dynamic effect value usually does not exceed 20% of the static load. Generally, the track can be modelled and simulated as a massless visco-elastic force, which means that both stiffness and damping of the rail are taken into account except for the inertia properties. The model adopts the following assumptions:

(1) Deformation of a track for different wheel sets are independent and can be computed separately;

(2) Deformations of the left and right tracks are independent;

(3) Track deformations include independent lateral, vertical deflections, corresponding to the track coordinate;

(4) Rail roll is not considered;

(5) The track would be modelled as a linear force element both in the lateral and vertical directions; the lateral dissipation is considered only for two-point contact model.

Employing the commercial software Universal Mechanism (short for UM) 7.2, the CRH2 combined with the CRTS III ballastless PC slab track model could be established using the related design parameters. The established multi-rigid-body dynamics model can be seen in Fig. 6.

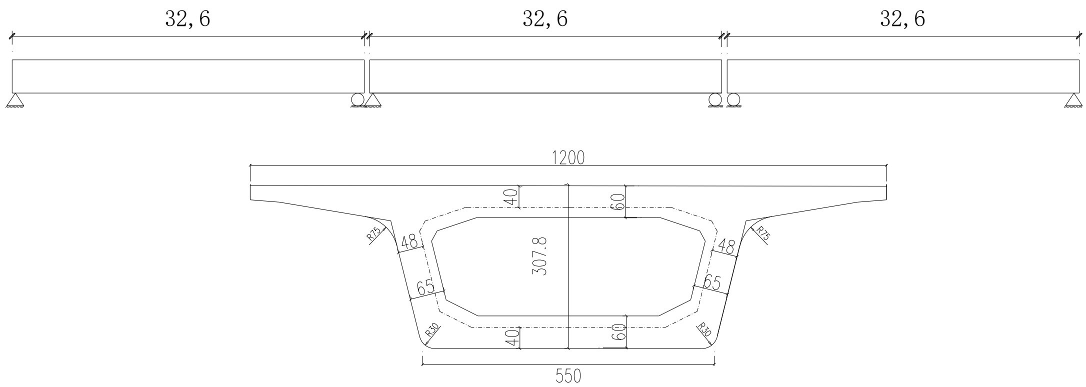

Fig. 7 (a) Support diagram of typical girder; (b) Cross section of typical 32 m-span girder (unit: cm)

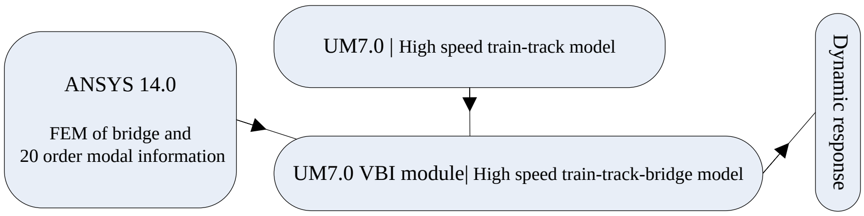

Fig. 8 Simulation process of train bridge dynamic interaction

Fig. 9 High-speed train-track-bridge simulation model

2.4 Bridge modelling

To conduct an accurate simulation of the working conditions of a high-speed railway, this paper employs a real bridge, the Yang Zhuang Bridge, as an example. Yang Zhuang Bridge consists of 3 successive simply supported pre-stressed concrete girders with 32 m-span lengths and box sections, which is one of the most common used types in the bridges of the Beijing-Shanghai high-speed railway. The support diagram and the cross section of the girders are shown in Fig. 7.

In this study, the 3-D finite element model was established according to the engineering drawings, created using ANSYS software. Both the bridge girders and the piers were modelled using a three-dimensional solid element (SOLID45). Then, the interface file of ANSYS and UM

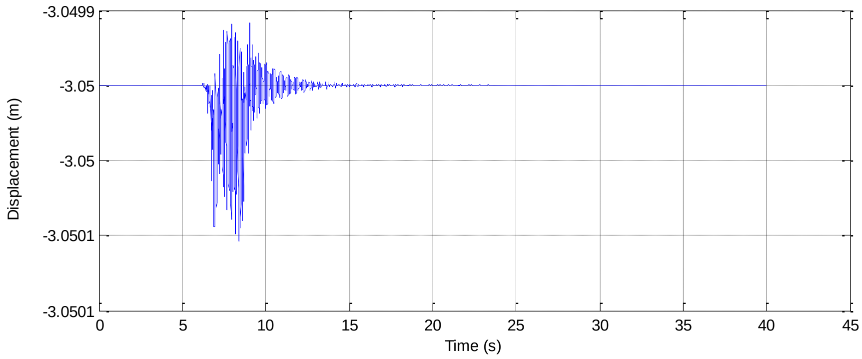

Fig. 10 Mid-span displacement curve of the 2nd span

was generated and the finite element model and selected model parameters could be loaded into the UM as flexible body. By calculating the train-track-bridge model in the VBI (Vehicle and Bridge Interaction) module, the dynamic responses including displacement, acceleration, velocity, stress, strain and other information could be obtained. The simulation process of train bridge dynamic interaction is shown in Fig. 8.

The high-speed train-track-bridge simulation model, multi-rigid-body dynamics model of train and track incorporating flexible body of the bridge, is shown in Fig. 9.

Fig. 10 shows the mid span displacement curve of the 2nd span in absolute coordinate system. It can be clearly seen from the figure that: (1) the high-speed train began to run on the bridge at *t*=6.5 s, meanwhile forced vibration of the bridge started; (2) from *t*=6.5 s to 9 s, the train was running on the train, and the obvious dynamic response peaks caused by vehicle were obtained; (3) after *t*=9 s, the train left the bridge and free vibration began and the bridge was allowed to vibrate without any other external dynamic excitation (for the high stiffness of the bridge, external excitations except for trains could hardly cause the bridge vibration). However, the displacement simulation results also indicated that the train induced displacement (no more than 0.1 mm at health status) is too small for the Structural Health Monitoring system at present. With the existing monitored equipment it is difficult to achieve high precision or such precision without rather expensive costs.

Generally, the Structural Health Monitoring (SHM) system could measure the environment and loads (temperature, humidity, wind, earthquake, vehicle loads etc.), global responses (acceleration, displacement etc.) and local responses (strain, cable force, corrosion, crack etc.). However, for the most commonly used, simply supported beam bridge, the scale of the SHM system might not be too large to include many monitored parameters. Therefore, the selection of monitored variables becomes extremely important to the safety evaluation of the bridge. Among all of these monitored parameters, the strain responses reflected the local and global properties, loading responses and the dynamic characteristics. In this study, the strain responses were selected as the monitored variable for easy testing, high precision and its relationship with the mechanical and dynamic properties of the bridge.

2.5 Damage simulation

According to the bridge inspection experience, the most easily damaged location of a simply

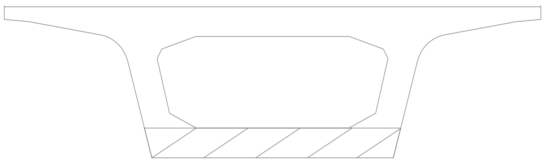

Fig. 11 Deterioration location of cross section

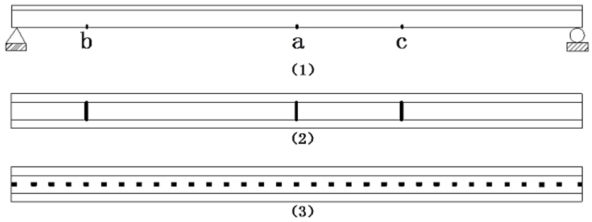

Fig. 12 Deterioration location of the bridge and sensor arrangement

Table 4 Stiffness degradation conditions

Working Condition	Specific Parameter Adjustment			
	Degradation location	*Stiffness degradation*	*Speed*	*Passenger loads*
I	a	5%, 10%, 15%, 20%, 25%, 30%, 35%, 40%, 45%, 50%	80m/s	Normal
II	b and c	5%, 10%, 15%, 20%, 25%, 30%, 35%, 40%, 45%, 50%	80m/s	Normal
III	a	10%, 20%, 30%, 40%, 50%	80m/s	Normal
		10%, 20%, 30%, 40%, 50%	60m/s	
IV	a	5%, 10%, 15%, 20%, 25%, 30%, 35%, 40%, 45%, 50%	80m/s	All full or partial load

supported beam bridge is the lower flange of the box girder. As a result, in this study, the stiffness deterioration would be simulated by decreasing the elastic modulus of the lower flange of the box girder, which was shown as the shadow part in Fig. 11. The second span of the simulated bridge (Fig. 9) was selected to simulate the stiffness degradation and the detailed deterioration location (The mid-span as section a, 4.3 m away from the fixed bearing as section b, 9.7 m away from the sliding bearing as section c as shown in Fig. 12 (1) and (2). Fig. 12 (3) shows the potential locations of monitored strain sensors.

To simulate the normal operating conditions, this paper considered four different types of working conditions, which were simulated by stiffness degradation degree and location changes, passenger number and train speed varying. The monitored simulated strain data could be employed for condition assessment of the bridge. The four working conditions were shown in Table 4.

Working condition I: for the second span, elastic modulus decreased from 5% to 50%; the stiffness degradation location was at section a; the train would pass through the bridge at a constant speed of 80 m/s and similar passenger loads;

Working condition II: for the second span, elastic modulus decreased from 5% to 50%; the stiffness degradation location was at sections b and c; the train would pass through the bridge at a constant speed of 80 m/s and similar passenger loads;

Working condition III: for the second span, elastic modulus decreased from 5% to 50%; the stiffness degradation location was at section a; the train would pass through the bridge at a different speed and similar passenger loads;

Working condition IV: for the second span, elastic modulus decreased from 5% to 50%; the stiffness degradation location was at section a; the train would pass through the bridge at a constant speed and different passenger loads; when the stiffness degradation is 25%, 35% and

45%, the passenger loads would be partial load, otherwise the passenger loads would be full load.

The working condition III were designated to investigate the velocity influence on the damage identification, while the working condition IV were used for studying the passenger loading influence.

3. Condition assessment methodology

3.1 Derivation of deflection from the monitored strain responses

For the condition assessment of the high-speed railway bridge, most of the existing design codes select vertical displacement and the natural frequency as the evaluation index. In this study, the dynamic strain response including train-bridge interaction stage and free vibration stage would be monitored by strain sensor. To evaluate the bridge condition using the design specification, the deflection curves would need to be deduced from the strain responses.

Relationship between displacement and strain

Based on the structural characteristics and mechanical properties of simply supported beam bridge, the relationship between the curvature and the sectional strain along the bridge can be expressed as

$$\frac{1}{\rho(x)} = \frac{d^2 y(x)}{dx^2} = \frac{\varepsilon(x)}{z(x)} \tag{4}$$

From Eq. (4), it can be seen that the deflection curve might be achieved by integral monitored strain responses $\varepsilon(x)$ and distance $z(x)$ at location x. However, in practical applications, the deflection derivation usually could not acquire satisfactory results for a limited number of strain sensors (Shin *et al.* 2012). Therefore, this study proposes a displacement derivation method based on constructing the displacement curve, where the undermined parameter could be optimized by the monitored strain responses.

Solution of displacement response

If a train with N wheel sets passed through a simply supported beam bridge (L, m and EI are the length of the bridge, the mass of per unit length and the bending stiffness, respectively) with constant velocity, the differential vibration equation of beam structure under external excitation can be expressed as

$$\begin{gathered} m\frac{\partial^2 y(x,t)}{\partial t^2} + c\frac{\partial y(x,t)}{\partial t} + EI\frac{\partial^4 y(x,t)}{\partial x^4} = \sum_{i=1}^{N} p_i \delta\left[x - v\left(t - t_i\right)\right] S\left[\frac{v\left(t-t_i\right)}{L}\right] \\ S\left(\xi\right) = \begin{cases} 1 & 0 \le \xi \le 1 \\ 0 & \text{else} \end{cases} \end{gathered} \tag{5}$$

where p_i and t_i represent the vehicle load of the i^{th} wheel sets and the time when the i^{th} wheel sets acted on the bridge; t indicates the operation time. The displacement response could be expanded in terms of modal contributions and expressed as the following formula

$$y(x,t)=\sum_{r=1}^{\infty}\phi_r(x)q_r(t)=\sum_{r=1}^{\infty}\sin\frac{r\pi x}{L}q_r(t) \tag{6}$$

The vibration of the bridge can be divided into two stages: when $0 \le t \le t_N + L/v$ (L_c indicates the length of the train) there are wheel sets acting on the bridge, the bridge suffered from forced vibration; when $t > t_N + L/v$, the last wheel sets have left the bridge, the bridge would vibrate freely (Li *et al.* 2012) to give the equation

$$y(x,t)=\sum_{r=1}^{\infty}\sin\frac{r\pi x}{L}\begin{Bmatrix} e^{-\xi_n\omega_n t}\left(A_n\cos\omega_{Dn}t+B_n\sin\omega_{Dn}t\right)+\dfrac{a_{0n}}{K_n} \\ +\dfrac{1}{K_n}\sum_{j=1}^{\infty}\left[A_{jn}\cos\left(j\theta t\right)+B_{jn}\sin\left(j\theta t\right)\right]\end{Bmatrix},0\le t\le t_N+L/v$$

$$y(x,t)=\sum_{r=1}^{\infty}\sin\frac{r\pi x}{L}\left\{e^{-\xi_n\omega_n\left(t-t_N-L/v\right)}\begin{bmatrix}A_{nn}\cos\omega_{Dn}\left(t-t_N-L/v\right)\\ +B_n\sin\omega_{Dn}\left(t-t_N-L/v\right)\end{bmatrix}\right\},t>t_N+L/v \tag{7}$$

Then, for the deflection responses at any fixed time $0 \le t \le t_N + L/v$, the deflection curve can be constructed by the following formulation for simplicity

$$y(x,t)=C+\sum_{r=1}^{\infty}a_r\sin\left(b_r x+c_r\right),0\le t\le t_N+L/v \tag{8}$$

where a_r, b_r, c_r and C were undetermined parameters. By substituting Eq. (11) to Eq. (5) and considering Eq. (4), the objective function $f_{obj}(x)$ gives

$$f_{obj}(x)=\frac{1}{\rho}-\frac{\varepsilon(x)}{z(x)}=\frac{d^2y}{dx^2}-\frac{\varepsilon(x)}{z(x)} \tag{9}$$

There would be $3\times r+1$ unknowns and n groups of measured strain value (n is the number of strain measurement locations, r was the modal expansion order); for the high order modal had limited contribution to the deflection curve, the modal order r=8 is selected in this study. Then, the parameters a_r, b_r and C in Eq. (11) can be determined by solving the optimization problem min$f_{obj}(x)$. Table 5 illustrates the evaluation indexes defined by different design specifications from different countries, which referred to the mid span displacement during forced vibration stage.

3.2 Damage identification based on train induced strain responses

The condition assessment of high-speed railway bridges employing specifications' rules shows certain limits because the derived displacement are not sensitive to the local stiffness degradation in practical application. Thus, the damage identification including stiffness degradation location and quantification needs to be directly identified by train induced strain responses.

Table 5 Evaluation indexes defined by different design specifications

Different design specifications	Indexes			
	frequency f_0		Maximum displacement d_{max}	
The new200km/h passenger and cargo collinear railway design regulations in China	$23.58L^{-0.592}$		$L/1200$	
The new 200-250km/h railway passenger dedicated design regulations in China	$23.58L^{-0.592}$		$L/1500$	
The new 300-350km/h railway passenger dedicated design regulations in China	$120/L$		$L/1500$	
Design standard and interpretation of railway structure in Japan	Speed V (km/h)	f_0	Speed V (km/h)	d_{max}
	≤ 210	$55L^{-0.8}$	260	$L/1200$
	$210<V\leq 300$	$70L^{-0.8}$	300	$L/1500$
	$260<V\leq 300$	$80L^{-0.8}$	360	$L/1900$
The high speed railway bridge regulations in Germany	$22.58L^{-0.592}$		$L/1700$	
UIC	$23.58L^{-0.592}$		$L/1500$	

Stiffness degradation location

Assumed that $\{\varepsilon_u\}$ and$\{\varepsilon_d\}$ were, respectively the strain response of the bridge at healthy and stiffness degradation status. For the high-speed railway bridge, the monitored strain responses for the first several years would be chosen as the foundation for safety evaluation under different EMU Marshalling and different train types. Then, the train responses monitored in the following years would be subtracted to the reference strain responses selected from the similar external excitations, demonstrated as $\Delta\varepsilon(j)=|\varepsilon_u(j)-\varepsilon_d(j)|$, where j indicates the monitored point. The parameter $\Delta\varepsilon(j)$ shows significant sensitivity to the local stiffness degradation. The more locations that strains were monitored, the more accurate damage identification results could be obtained. Because the stiffness degradation was a gradual process, the strain response subtraction when the same axle of the similar train passed through the same location on the bridge, the stiffness degradation characteristics would be more evident.

Stiffness degradation quantification

Through simple strain subtraction, the stiffness degradation locations, where there were significant strain changes under similar external train excitation, could be identified in the previous section. The corresponding strain sensor number i could be easily and accurately marked for the damage location reference.

For the dynamic strain response at free vibration stage, this paper conducted strain modal analysis for obtaining the modal frequencies and strain modal shape $\boldsymbol{\varphi}_r=[\varphi_{1r}, \varphi_{2r},..., \varphi_{ir},..., \varphi_{nr}]$. The identified stain mode shape would be normalized by a reference value φ_b, which can be expressed as

$$\{\phi_{1r,}\phi_{2r,},...,\phi_{ir,}...\phi_{nr,}\} \Rightarrow \left\{\frac{\varphi_{1r}}{\varphi_{br}},\frac{\varphi_{2r}}{\varphi_{br}},...,\frac{\varphi_{ir}}{\varphi_{br}},...,\frac{\varphi_{nr}}{\varphi_{br}}\right\}$$

where r represents the modal order; n indicates the total number of strain sensors. The stiffness degradation index β_{ir} is defined as follows

$$\beta_{ir} = \frac{\phi_{ir}^{*} - \phi_{ir}}{\phi_{ir}} * 100\%$$

where ϕ_{ir}^{*} indicates the modal shape value of high-speed railway bridge at the stiffness degradation status. The defined parameter β_{ir} and the degree of stiffness degradation had certain relations and can be reduced to simple equations for high-speed railway bridge, which is demonstrated in the following case study in detail.

4. Results and discussion

4.1 Strain response data

As the train passes through the bridge, the high-speed train-track-bridge interaction system could generate a dynamic response. In this paper, the coupled train-track-bridge model was simulated in the VBI module of UM to generate the strain response and deflection, where strain responses were assumed to be monitored variable. For the four above-mentioned working conditions, the starting time for event trigger monitoring is set to the time when the monitored train is 500 m away from the bridge. The monitored time length is 40 s with 400 Hz sampling frequency. Fig. 13 shows the mid span strain time history at the lower flange of the girder for working condition 1. The same phenomenon and characteristics could be observed from the strain time history and above displacement time history.

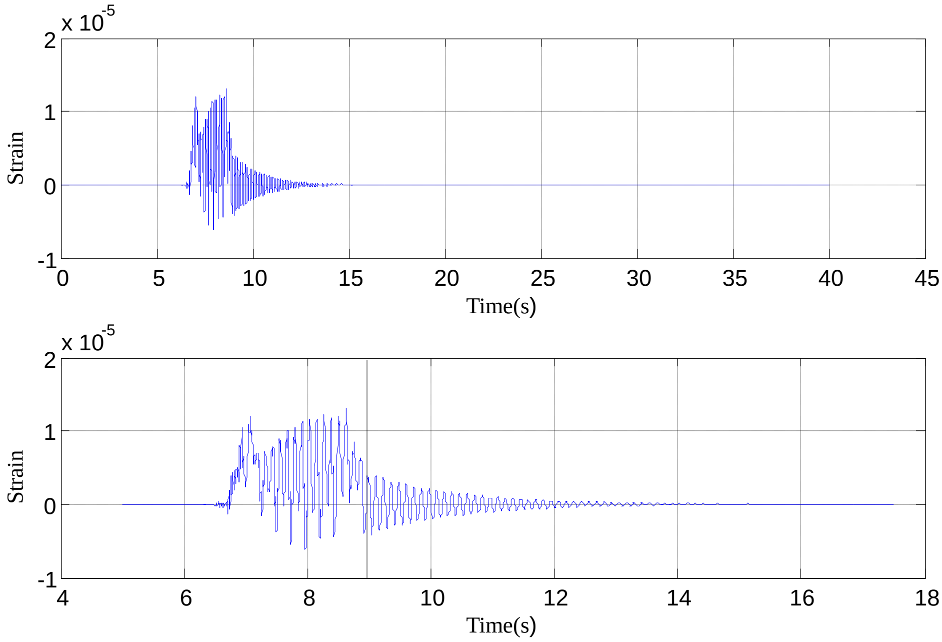

Fig. 13 Mid Span strain time history of the 2nd span

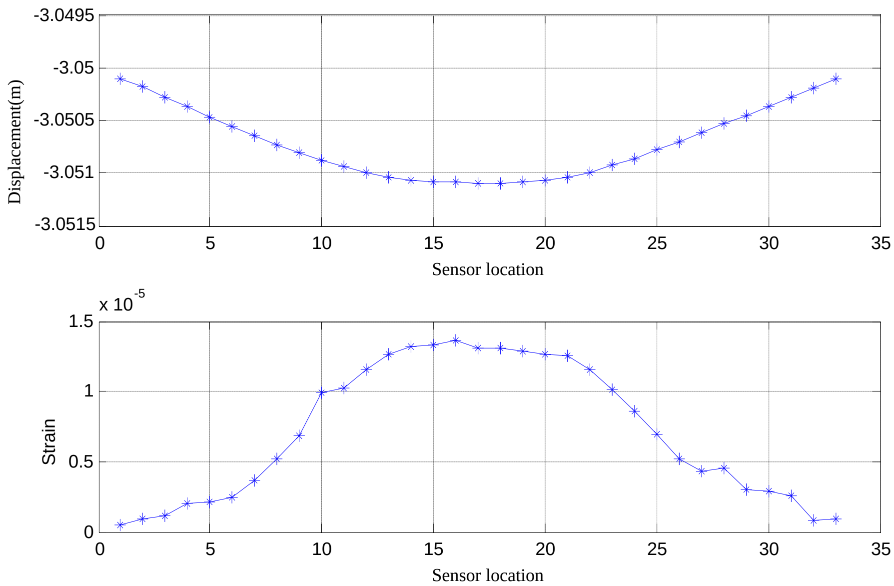

Fig. 14 Maximum deflection and strain curve along the bridge at *t*=8.36 s

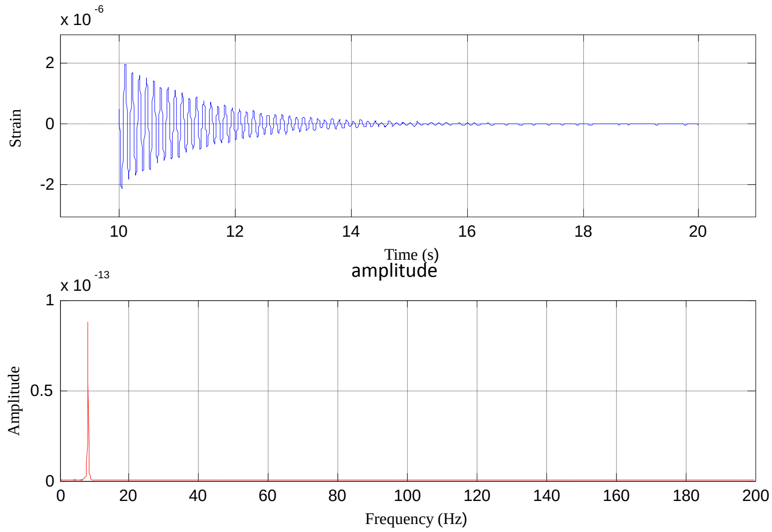

Fig. 15 Strain response data at the free vibration stage and FFT results

The strain response data under different conditions can reflect different characteristics: at the forced vibration stage, the response amplitude is relatively large and strain data mainly reflects the mechanical properties of the bridge; at the free vibration stage after the train passed through the bridge, strain data shows the dynamic properties clearly. Fig. 14 gives the maximum deflection and strain curve along the bridge when the mid span strain reached its maximum value (*t*=8.36 s).

Fig. 15 illustrates the strain responses at the free vibration stage. The natural frequencies were identified by the strain response data using a fast Fourier transform method. The identified frequency was 8.158 Hz for the bridge at health status.

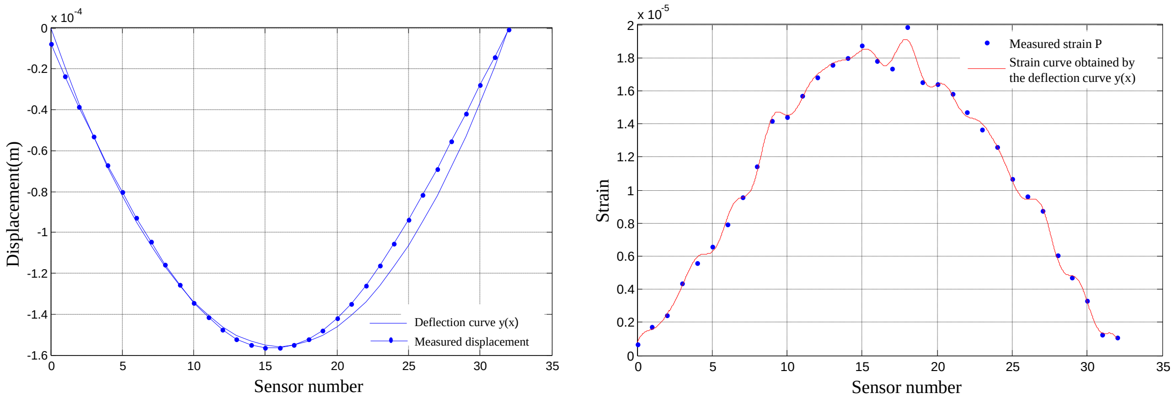

Fig. 16 Comparison of derived and the numerical simulated (a) displacement and (b) strain responses

4.2 Condition assessment based on derived deflection

The deflection curve was deduced by the proposed strain to response derivation method. Fig. 16(a) illustrates the comparison between calculated and strain derived displacement response. Fig. 16(b) gives the comparison of strain responses and two order differential of derived displacement, showing that the proposed method could generate precise displacement results based on monitored strain responses.

The response data of the four working conditions were shown in Table 6. It could be seen form Table 6 that the natural frequencies at four working conditions were much higher than the specification-defined frequency f=80L$^{-0.8}$=5 Hz. The maximum vertical deflections of mid-span were also much smaller than the specifications defined L/1700=0.0189 m.

Table 6 Identified frequencies and deflection for the four working conditions

Working condition I						Working condition III					
Degree 80 m/s	f (Hz)	d_{max} (mm)	Degree 80 m/s	f (Hz)	d_{max} (mm)	Degree 60 m/s	f (Hz)	d_{max} (mm)	Degree 80 m/s	f (Hz)	d_{max} (mm)
5%	8.157	1.806	30%	8.143	1.825	10%	8.153	1.806	10%	8.153	1.812
10%	8.153	1.812	35%	8.139	1.831	20%	8.150	1.812	20%	8.150	1.819
15%	8.153	1.814	40%	8.134	1.837	30%	8.143	1.824	30%	8.143	1.825
20%	8.150	1.819	45%	8.128	1.838	40%	8.134	1.831	40%	8.134	1.837
25%	8.147	1.823	50%	8.123	1.852	50%	8.123	1.843	50%	8.123	1.852
Working condition II						Working condition IV					
Degree 80 m/s	f (Hz)	d_{max} (mm)	Degree 80 m/s	f (Hz)	d_{max} (mm)	Degree	f (Hz)	d_{max} (mm)	Degree	f (Hz)	d_{max} (mm)
5%	8.156	2.826	30%	8.142	2.939	5%	8.157	1.993	30%	8.143	2.024
10%	8.154	2.858	35%	8.138	2.988	10%	8.153	1.998	35%	8.139	2.035
15%	8.151	2.887	40%	8.133	2.994	15%	8.153	2.002	40%	8.134	2.041
20%	8.148	2.902	45%	8.128	3.002	20%	8.150	2.010	45%	8.128	2.042
25%	8.145	2.921	50%	8.122	3.043	25%	8.147	2.018	50%	8.123	2.043

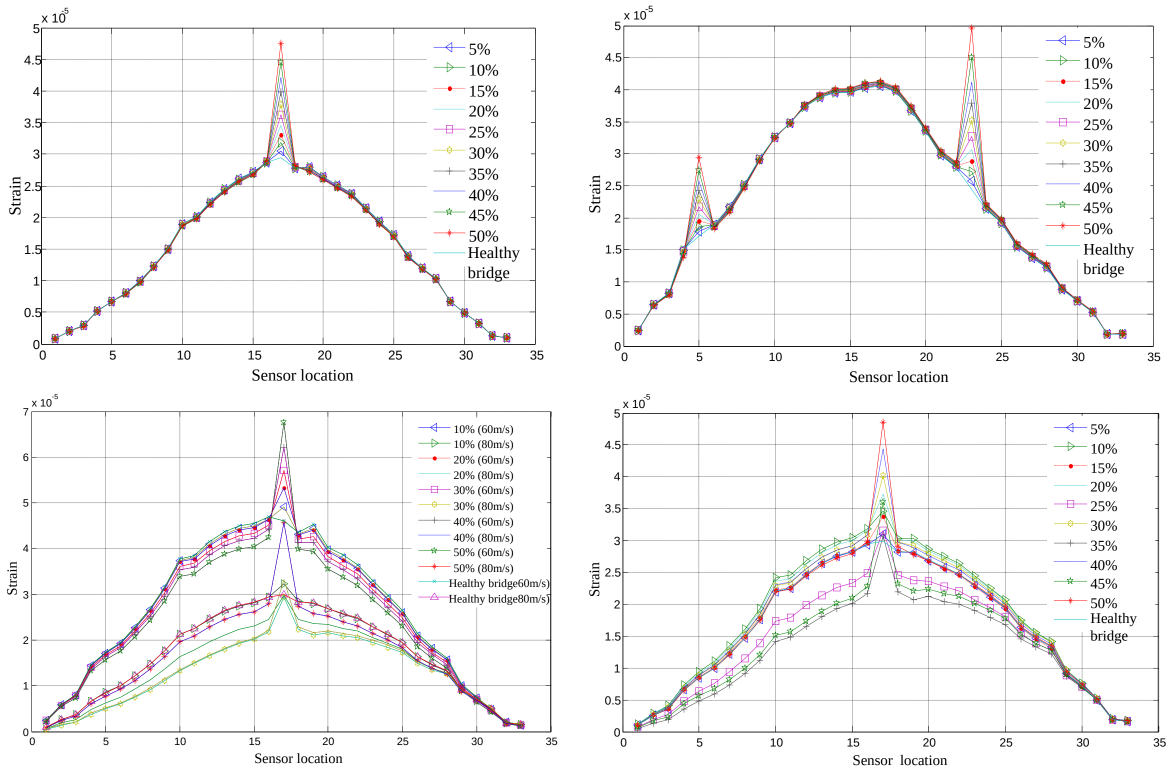

Fig. 17 Maximum strain response of the whole span for working condition (a) I; (b) II; (c) III; (d) IV

From the regulations comparison, under the local stiffness degradation status, even under very serious situations (50% stiffness deterioration), the identified mechanical and dynamic indexes were still fulfilling the specification requirements. The displacement and the frequencies show limited sensitivity to the local stiffness degradation and the displacement is not the ideal monitoring variable for a small span high-speed railway bridge. The condition assessment based on the specifications method resulted in difficult to identification of the potential problems in high-speed railway bridge with high stiffness and could not provide basis and guidance for repair and maintenance decision.

4.3 Stiffness degradation location identification

This paper directly uses the strain response data to locate the stiffness degradation of the bridge based on the strain data accumulation under similar external excitations. Fig. 17 shows the maximum strain curve for the whole span of the four working conditions, the occurrence of which are different for different operation speed. It could be seen from the figure that the strain increased dramatically at the stiffness degradation location but remained steady at the other places. Such remarkable features of the strain data could help a researcher find an effective and simple methodology for positioning stiffness degradation locations. Fig. 17(c), (d) also show that the operation speed and the passenger weight have certain influence on the strain responses. The higher the operation train speed and passenger weights, the higher dynamic interaction strain

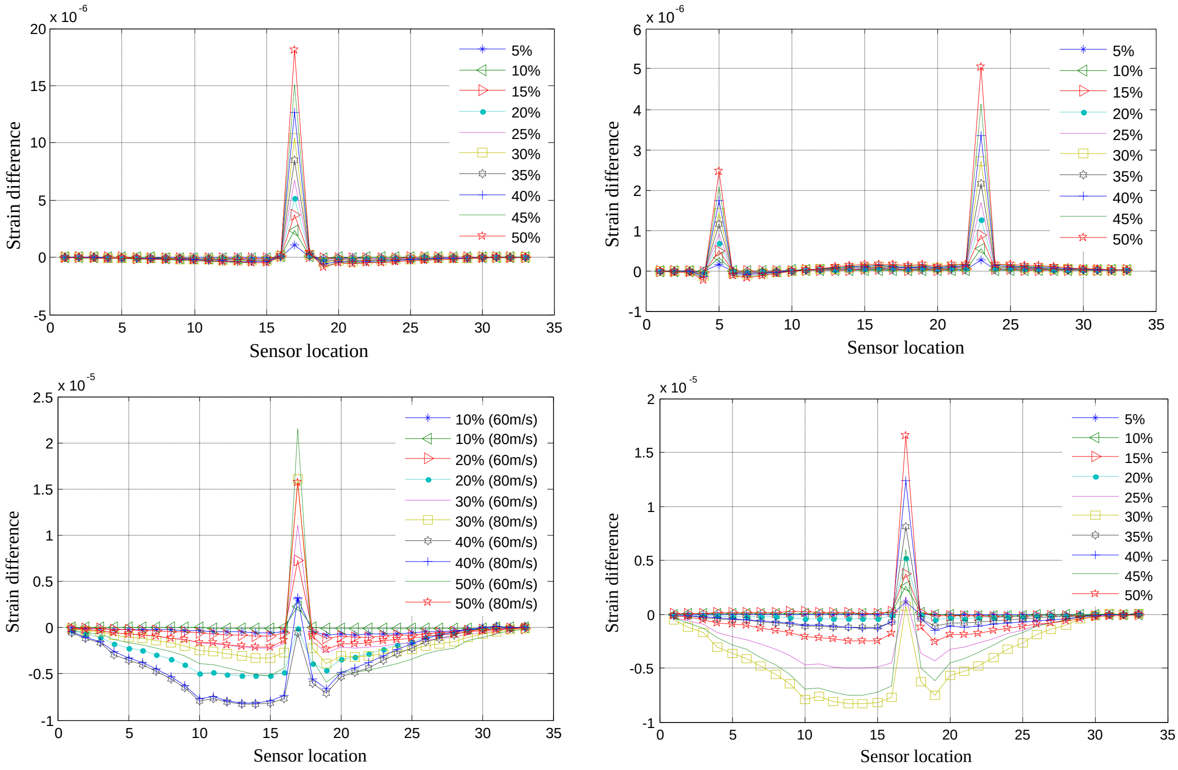

Fig. 18 Stiffness degradation location for working condition (a) I; (b) II; (c) III; (d) IV

responses.

Based on the strain subtraction between healthy and deterioration status $\Delta\varepsilon(j)$, Fig. 18 illustrates the stiffness degradation location for four working conditions. It could be seen from Fig. 18 (a), (b) that for working conditions I & II with the same passenger weight and train speed, the proposed subtraction method could quickly and correctly locate single or multiple occurrences of stiffness degradation. For working conditions III & IV (Fig. 18(c), (d)), the subtraction could also be used to identify the damage degradation location. However, the strain differences were relatively large at certain monitoring points.

The usage of proposed stiffness degradation location method has several prerequisite:

(1) Massive strain data needs to be monitored during normal operation conditions. The more data monitored, the accurate location identification results;

(2) The strain data acquiring by SHM system needs to be stored with certain feathers, such as operation speed and passenger number etc. The subtraction should be done between two trains under similar external excitations.

4.4 Stiffness degradation degree identification

To validate the effectiveness of the proposed stiffness degradation method, more working conditions need to be simulated as shown in Table 7. Seen from Table 7, the simulation includes single and multiple stiffness degradation conditions. Due to the high rigidity characteristics and

Table 7 Stiffness degradation working conditions

	Single degradation				Multiple degradation			
Working Condition	V	VI	VII	VIII	IX	X	XI	XII
Location (m)	4.3	12.3	16.3	22.3	4.3, 22.3	12.3, 26.3	4.3, 12.3, 26.3	8.3, 12.3, 23.3

excellent integrity performance, the higher order modes are difficult to excite; and therefore, the first mode would be the identified mode under most circumstances.

For Working Condition V, the strain subtraction results illustrated in Fig. 19. It could be seen in Fig. 19 that the fifth strain sensor (at location 4.3 m) shows the dramatic increasing trend and could accurately locate the stiffness degradation. After the damage degradation location, the stiffness degradation index β_5 could be calculated using the free vibration strain. The relationship between the stiffness degradation index β_5 and the stiffness degradation degree α is shown in Fig. 20. The scatter in Working Condition V could be fitted by quadratic function as follows

$$\beta = 0.02501\alpha^2 + 0.568\alpha + 2.718 \tag{10}$$

The correlation coefficient is as high as 0.9994, showing higher linear relationship between damage index and damage degree for Working Condition V. Fig. 20(b) shows the damage degree between working conditions V-XII and the corresponding damage indexes. The above fitted quadratic function also shows an excellent linear relationship (correlation coefficient 0.9642), indicating that no matter where damage degradation occurs, the degradation degree could be identified using the fitted quadratic function by damage index β. The damage at different locations shows limited correlation between each other, and the damage degree could be generated from the quadratic function separately using the calculated β at different locations.

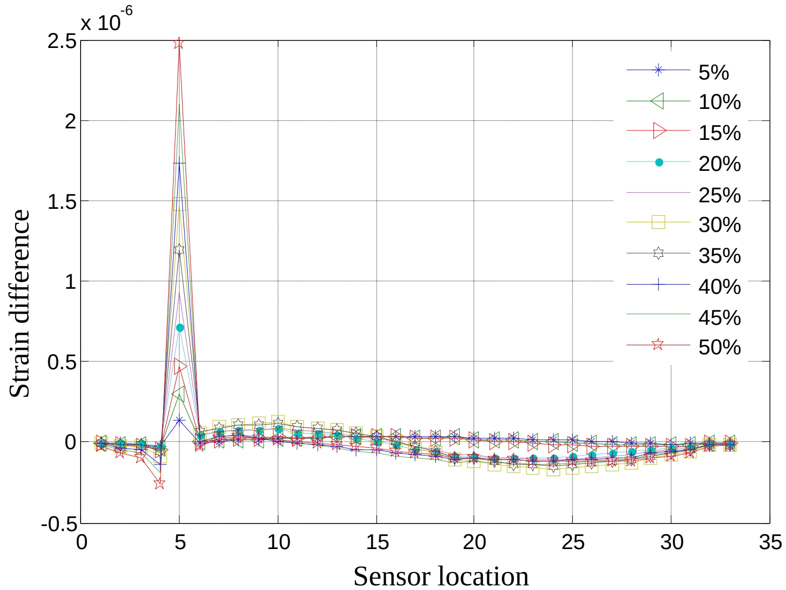

Fig. 19 Stiffness degradation location for working condition V

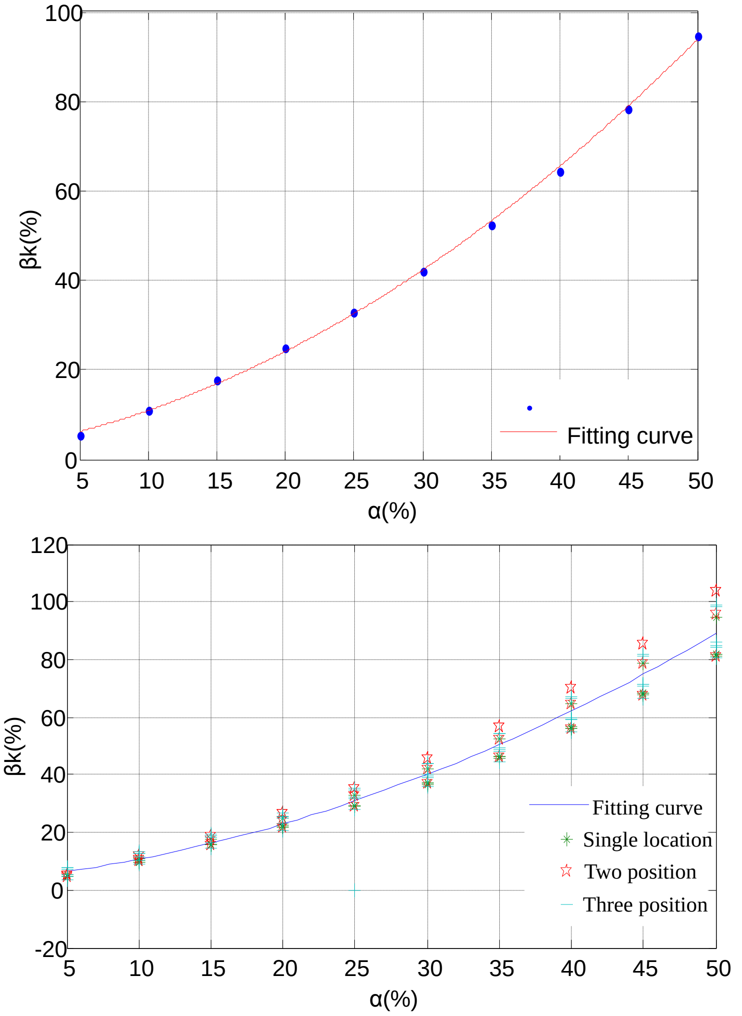

Fig. 20 Relationship between the stiffness degradation index and the stiffness degradation degree

In this study, measurement error and modelling error are not considered. The influence of such errors to the damage identification results might be investigated in the near future.

5. Conclusions

This paper presents the condition assessment method of high-speed railway bridge, locating and assessing stiffness degradation of the bridges. The following conclusions could be drawn from the results of study:

(1) For high rigidity of high-speed railway bridge, the strain response was proven to be the ideal monitoring variable. Strain responses are composed of two parts: train-train-bridge dynamic interaction response and free vibration response, reflecting both mechanical and dynamical properties of the mostly used simply support Beam Bridge. The strain derived deflection and the

frequencies show limited sensitivity to the local stiffness degradation and the condition assessment based on the specification indexes is not very applicable.

(2) Based on the massive strain response data monitored by the SHM system, the stiffness degradation location could be easily identified by the subtraction of strain responses between health status and damage status under similar selected external excitations considering limited vehicle types of high-speed railway.

(3) After the stiffness degradation location, for the high-speed rail way bridge, the damage degree and proposed damage index could be fitted by quadratic function. The damage degree could be calculated from the strain modal shape difference, which could be identified by the free strain vibration of the bridge.

Acknowledgements

The research described in this paper was financially supported by the Natural Science Foundation of China (Grant No. 51478149), MOST (Grant No. 2011BAK02B02, 2011CB013604, 2013CB036305).

References

Adam, C. and Salcher, P. (2014), "Dynamic effect of high-speed trains on simple bridge structures", *Struct. Eng. Mech.*, **51**(4), 581-599.

Arvidsson, T., Karoumi, R. and Pacoste, C. (2014), "Statistical screening of modelling alternatives in train-bridge interaction systems", *Eng. Struct.*, **59**, 693-701.

Banjara, N.K. and Sasmal, S. (2014), "Remaining fatigue life of steel railway bridges under enhanced axle loads", *Struct. Infrastruct. Eng.*, **10**(2), 213-224.

Brühwiler, E., Bosshard, M., Steck, P., Meyer, C., Tschumi, M. and Haldimann, S. (2013), "Fatigue safety examination of a riveted railway bridge using data from long term monitoring", *Proceedings of the IABSE Symposium Report, International Association for Bridge and Structural Engineering*, 477-484.

Kim, C.W., Kawatani, M., Lee, C.H. and Nishimura, N. (2007), "Seismic response of a monorail bridge incorporating train-bridge interaction", *Struct. Eng. Mech.*, **26**(2), 111-126.

Kim, D.K., Yu, S.Y. and Choi, H.S. (2013), "Condition assessment of raking damaged bulk carriers under vertical bending moments", *Struct. Eng. Mech.*, **46**(5), 629-644.

Klasztorny, M. (2001), "Vertical vibrations of a multi-span beam steel bridge induced by a superfast passenger train", *Struct. Eng. Mech.*, **12**(3), 267-281.

Liu, K., De Roeck, G. and Lombaert, G. (2009), "The effect of dynamic train-bridge interaction on the bridge response during a train passage", *J. Sound Vib.*, **325**(1-2), 240-251.

Li, X.Z., Zhang, Z.J. and Liu, Q.M. (2012), "Vertical dynamic response analysis of a simply supported beam bridge under successive moving loads", *Zhendong yu Chongji (Journal of Vibration and Shock)*, **31**(20), 137-142.

Niu, B. (2008), "Review of high speed railway bridges in China", *Proceedings of the 18th National Bridge Academic Conference*, Tianjin, China, June.

Podworna, M. (2011), "Dynamics of a bridge beam under a stream of moving elements. Part 1-Modelling and numerical integration", *Struct. Eng. Mech.*, **38**(3), 283-300.

Podworna, M. (2011), "Dynamics of a bridge beam under a stream of moving elements. Part 2-Numerical simulations", *Struct. Eng. Mech.*, **38**(3), 301-314.

Shin, S., Lee, S.U., Kim, Y. and Kim, N.S. (2012), "Estimation of bridge displacement responses using FBG

sensors and theoretical mode shapes", *Struct. Eng. Mech.*, **42**(2), 229-245.
Rezvani, M.A., Vesali, F. and Eghbali, A. (2013), "Dynamic response of railway bridges traversed simultaneously by opposing moving trains", *Struct. Eng. Mech.*, **46**(5), 713-734.
Shu, J.P., Zhang, Z.Y., Gonzalez, I. and Karoumi, R. (2013), "The application of a damage detection method using Artificial Neural Network and train-induced vibrations on a simplified railway bridge model", *Eng. Struct.*, **52**, 408-421.
Song, M.K. and Fujino, Y. (2008), "Dynamic analysis of guideway structures by considering ultra high-speed Maglev train-guideway interaction", *Struct. Eng. Mech.*, **29**(4), 355-380.
Sousa, C., Calçada, R. and Neves, A. (2008), "Fatigue life of precast decks of high speed railway bridges", *Proc., Life-Cycle Civil Engineering: Proceedings of the International Symposium on Life-Cycle Civil Engineering, IALCCE'08*, Varenna, Lake Como, Italy, June.
Sousa, C., Rocha, J.F., Calcada, R. and Neves, A.S. (2013), "Fatigue analysis of box-girder webs subjected to in-plane shear and transverse bending induced by railway traffic", *Eng. Struct.*, **54**, 248-261.
Vieira, R.F., Lisi, D. and Virtuoso, F.B. (2014), "Dynamic analysis of bridge girders submitted to an eccentric moving load", *Struct. Eng. Mech.,* **52**(1), 173-203.
Xia, H. and Zhang, N. (2005), "Dynamic analysis of railway bridge under high-speed trains", *Comput. Struct.*, **83**(23-24), 1891-1901.
Xia, H., Deng, Y., Xia, C., De Roeck, G., Qi, L. and Sun, L. (2013), "Dynamic analysis of coupled train-ladder track-elevated bridge system", *Struct. Eng. Mech.*, **47**(5), 661-678.
Yang, H.Y., Chen, Z.J., Zhang, H.L. and Fan, J.P. (2014), "Dynamic analysis of train-rail-bridge interaction considering concrete creep of a multi-span simply supported bridge", *Adv. Struct. Eng.*, **17**(5), 709-720.
Zhang, N., Xia, H. and Guo, W.W. (2008), "Vehicle-bridge interaction analysis under high-speed trains", *J. Sound Vib.*, **309**(3-5), 407-425.
Zhan, J.W., Xia, H., Chen, S.Y. and De Roeck, G. (2011), "Structural damage identification for railway bridges based on train-induced bridge responses and sensitivity analysis", *J. Sound Vib.*, **330**(4), 757-770.
Zhao, M. and Di, J. (2014), "Fatigue load for cable-girder anchorage structure of highway and light-railway cable stayed bridge", *Civil, Structural and Environmental Engineering, Pts 1-4*, Eds. X. Zhang, B. Zhang, L. Jiang, and M. Xie, 1028-1033.